MASTER OSCILLATOR TECHNIQUES FOR 10 MICRON RADAR

A. Stein

United Aircraft Research Laboratories

Prepared for:

Office of Naval Research
Advanced Research Projects Agency

30 September 1973

M921512-5

Semi-Annual Technical Report

Master Oscillator Techniques For 10 Micron Radar

by

A. Stein
United Aircraft Research Laboratories
East Hartford, Connecticut 06108
(203) 565-4341

September 30, 1973

Prepared for the Office of Naval Research
Scientific Contracting Officer-Dr. M. White
Contract N00014-73-C-0086 - $122,664.00
25 August 1972 to 31 December 1973

Sponsored by
Advanced Research Projects Agency
ARPA Order 1806, Amendment No. 6, 7-18-72

TABLE OF CONTENTS

LIST OF ILLUSTRATIONS

SUMMARY

A CO_2 waveguide laser was coupling-modulated with the help of an intracavity electro-optic polarization switch. Linear FM-modulation was achieved by sweeping the drive frequency from 100 to 500 MHz in linear fashion. The optical beam coupled from the resonator represented a suppressed-carrier-double-sideband-modulated signal. The sidebands are chirped in opposite spectral directions as the modulation is swept through the chirp range. By placing the optical carrier in the wing of the P(20) gain profile, only one sideband chirps through the range of interest, the other falls outside the gain profile.

This experiment represents a further important step towards the contract goal to obtain fast linear FM-modulation centered on the P(20) line profile. The resonator length and the pressure of the active gas (i.e., the gain-bandwidth) are chosen such that only two axial optical modes exist within the active range of the gain profile. Fine adjustment of the resonator length is employed to tune these two modes to a symmetrical position relative to the gain profile. One resonator mirror is replaced by a combination of a semitransparent mirror and a diffraction grating in Littrow alignment. The grating provides a coarse frequency discrimination selecting the desired molecular transition. Furthermore, together with the semitransparent element, the grating forms an interferometer whose effective reflectivity varies on a fine scale in accordance with the characteristic of a Fabry-Perot filter which is tuned to yield a minimum of reflection at one of the two axial resonances of the main resonator, thus suppressing that mode.

If the frequency excursion of the sidebands is sufficiently large, energy is coupled from the active mode into the suppressed neighboring resonance. One of the essential tasks of this program is to determine the response of the suppressed mode at the instance of coupling. During the reporting period, the mode-controlled system was assembled and partially tested. Clean line selection was achieved.

A second important result obtained during the reporting period is the design, construction and testing of a sealed-off CO_2 waveguide laser which is to yield the required frequency stability. Capillary opening, fill pressure and gas composition were varied to optimize the output power. For a 1.5 mm ID, 12.5 cm long BeO capillary at 20°C we measured an output power of 1.5 W at 100 torr pressure.

2.0 BACKGROUND

A stable master oscillator is required for application in a high resolution optical radar, currently under development at MIT's Lincoln Laboratory, which employs simultaneous measurement of both differential range and doppler to obtain three-dimensional mapping of distant, spinning objects. In analogy to existing equivalent microwave radar techniques, a number of different waveforms are of interest. The ultimate choice of waveform is governed by the performance of the available laser hardware; i.e., the master oscillator, power amplifier and local oscillator elements.

It is worth noting that Lincoln Laboratory's radar waveform design (discussed in the previous semi-annual report on this contract) underwent a revision in keeping with the development of laser power amplifiers (Ref. 1). The new waveform consists of a constant amplitude pulse of 5 (10) msec duration during which the optical frequency is swept 1500 (3000) times through a 500 MHz range (see Fig. 1). Each chirp has a duration of 3.1 μsec after which the frequency is quickly returned (0.2 μsec fly-back time) to its initial value and the chirp process is repeated. The chirp is to be linear with time within an accuracy of better than 300 kHz and initiation of the frequency ramp is locked to a precise clock circuit to better than 1 nsec.

Several different master oscillator designs have been proposed. One such system, for instance, employs external modulation in which the laser beam is propagated through an electro-optical crystal driven by a frequency-swept rf-field to generate sidebands to the optical carrier which exhibit the required frequency chirping. To center the frequency ramp on the peak of the P(20) line, one must offset the optical carrier frequency accordingly. There are again several proposed solutions to this problem. The master oscillator may, for instance, be a CO_2 isotope system which yields a transition (and hence carrier frequency) displaced from the P(20) line of the standard $^{12}C^{16}O_2$ 001 - $10^0$0 transition (Ref. 1). The center frequency of the modulating signal is then chosen equal to the difference in frequency between the two transitions such that one sideband falls inside the P(20) line profile.

One may also use a wide-band master oscillator operating in the P(20) line provided that appropriate mode selection is implemented such as to obtain oscillation in a single mode (the carrier) at the desired spectral displacement from line center.

While external modulation has the advantage of separating the problems of modulation and stabilization, it suffers from inefficiency since only a fraction of the incident optical power is coupled into the sideband of interest. It is for this reason that our investigation has focused on intracavity modulation techniques since they offer, in principle, significantly larger modulation efficiencies.

NEW RADAR WAVEFORM

f_O = CENTER OF P(20) LINE OF $00^0 1 \rightarrow 10^0 0$ CO_2 LASER TRANSITION

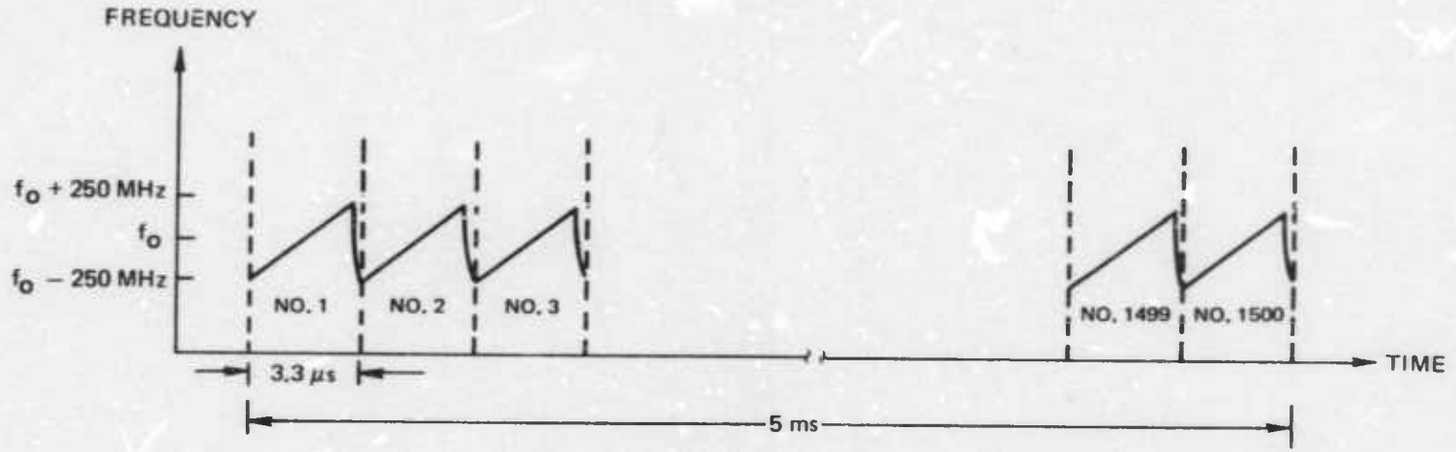

FIG. 1

(A linear frequency chirp can also be obtained by varying the optical length of the resonator with the help of an intracavity electro-optic crystal. This technique, however, is limited to moderate bandwidths, since the chirp range cannot exceed the intermodal frequency difference or the gain bandwidth.)

A modulation scheme which is not limited in bandwidth either by the c/2L value or the gain profile is called coupling modulation and makes use of electro-optic polarization switching. Here, the polarization vector is moved about a null position by an external voltage. For a sinusoidal drive that motion is also sinusoidal and the resulting optical signal is of mixed polarization. In the dominant polarization, we find the carrier at f and sidebands at $f \pm 2fm$ (see Fig. 2). In the orthogonal polarization, we find two sidebands, $f \pm f_m$, while the carrier is suppressed. (See Appendix A for a discussion of coupling modulation and Appendix B for an analysis on modulation distortion due to tolerances in the crystal alignment.) To obtain the required chirp signal, one sweeps the modulation frequency and separates one of the sidebands from the other. This can be achieved by appropriate frequency control prior to application of the modulating signal. By precise adjustment of the resonator spacing and simultaneous suppression of all but one axial mode, one may tune the frequency of the selected oscillating mode to the side of the gain profile of the active molecular transition. When the modulation is applied, both sidebands sweep in opposite spectral direction. This procedure in itself does not separate the two chirped sidebands; but if the oscillator output is fed into an amplifier system, also employing the P(20), $00^01 - 10^00$ transition, the separation becomes effective. One sideband is chirped symmetrically through the amplifier gain profile while the other sweeps away from the active line. To be precise, one should define a degree of separation stating the relative intensity of the sidebands after amplification.

The isolation is enhanced if the modulation frequency is swept between two high-frequency values, say from 100 to 600 MHz rather than from dc to 500 MHz.

To implement the required carrier offset, we use a wide-band oscillator, specifically a waveguide laser, whose active transition is collision broadened to 1 GHz bandwidth at 200 torr gas pressure. Carrier offset and mode selection is obtained by using a three-mirror resonator as shown in Fig. 3.

The distance of M_2 from the capillary is equal to its radius of curvature such that the optical wave emerging from the waveguide is refocused back into the guide where it propagates to the other opening and is collimated by the lens, reflected by M_1 and focused backinto the waveguide. Provided the gain exceeds the transmission loss and other resonator losses, this structure permits stable oscillation. To obtain the necessary mode selection, one must lower the optical feedback selectively; we use a third reflective element which forms a Fabry-Perot interferometer with M_1 and yields low reflectivity for certain narrow frequency ranges while maintaining a high reflectivity everywhere else. The third reflective element is a Littrow diffraction grating which aside from forming part of the Fabry-Perot filter provides sufficient discrimination against all but the P(20) transition. Figure 4 illustrates the mode selection provided by the Fabry-Perot.

FIG. 2

UARL WAVEGUIDE CO_2 LASER

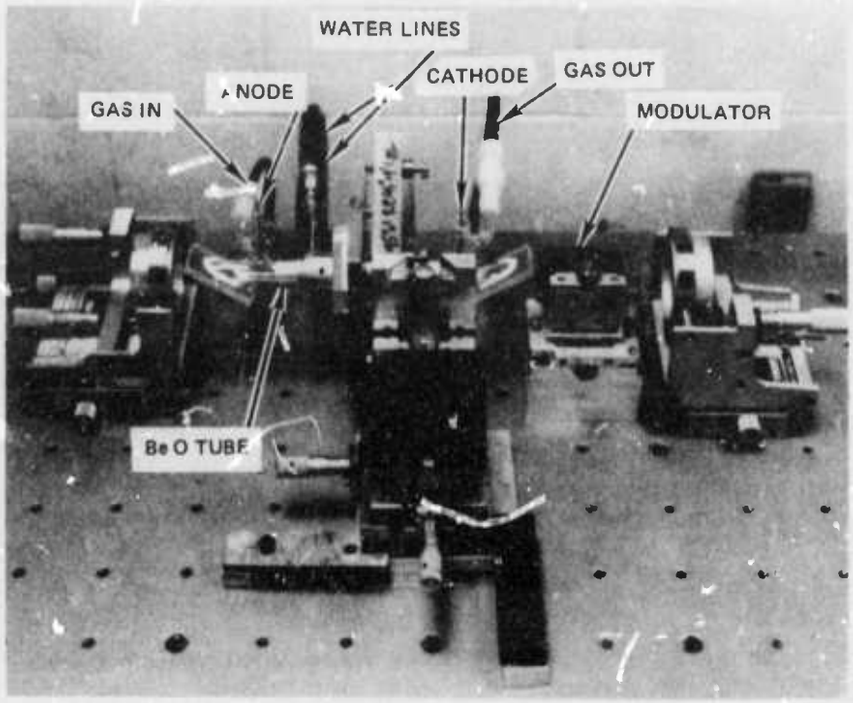

RL 73–57

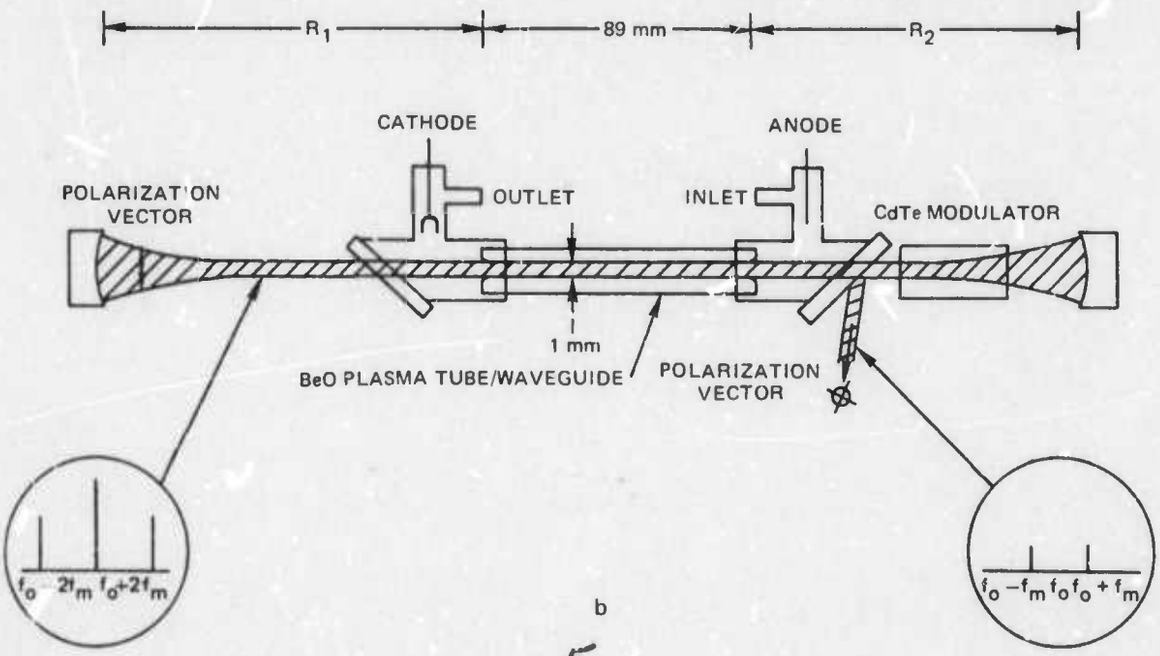

b

WGL WITH MODE AND LINE SELECTION

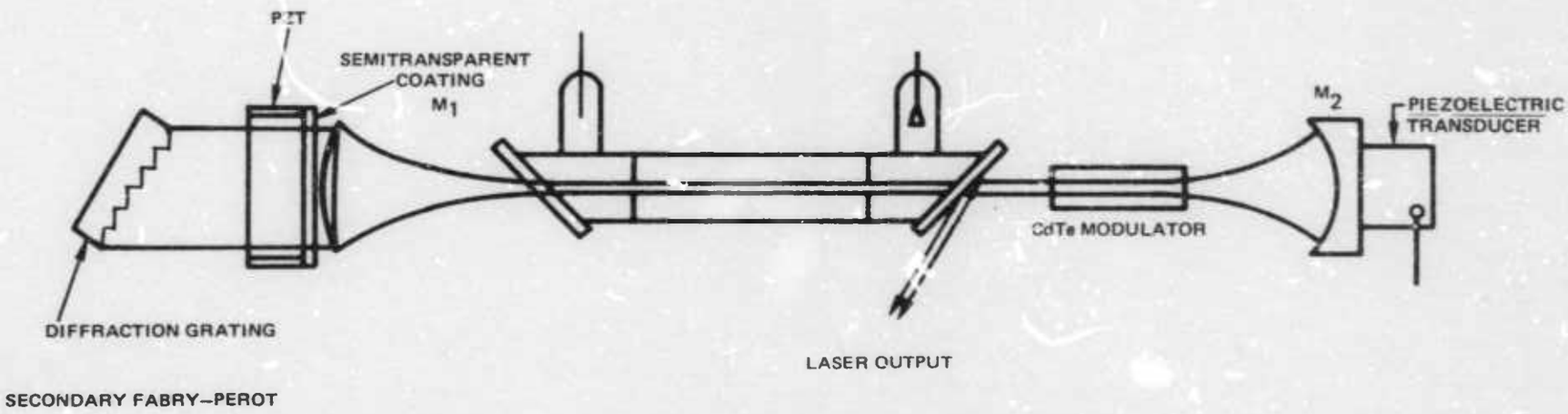

FIG. 3

FIG. 4

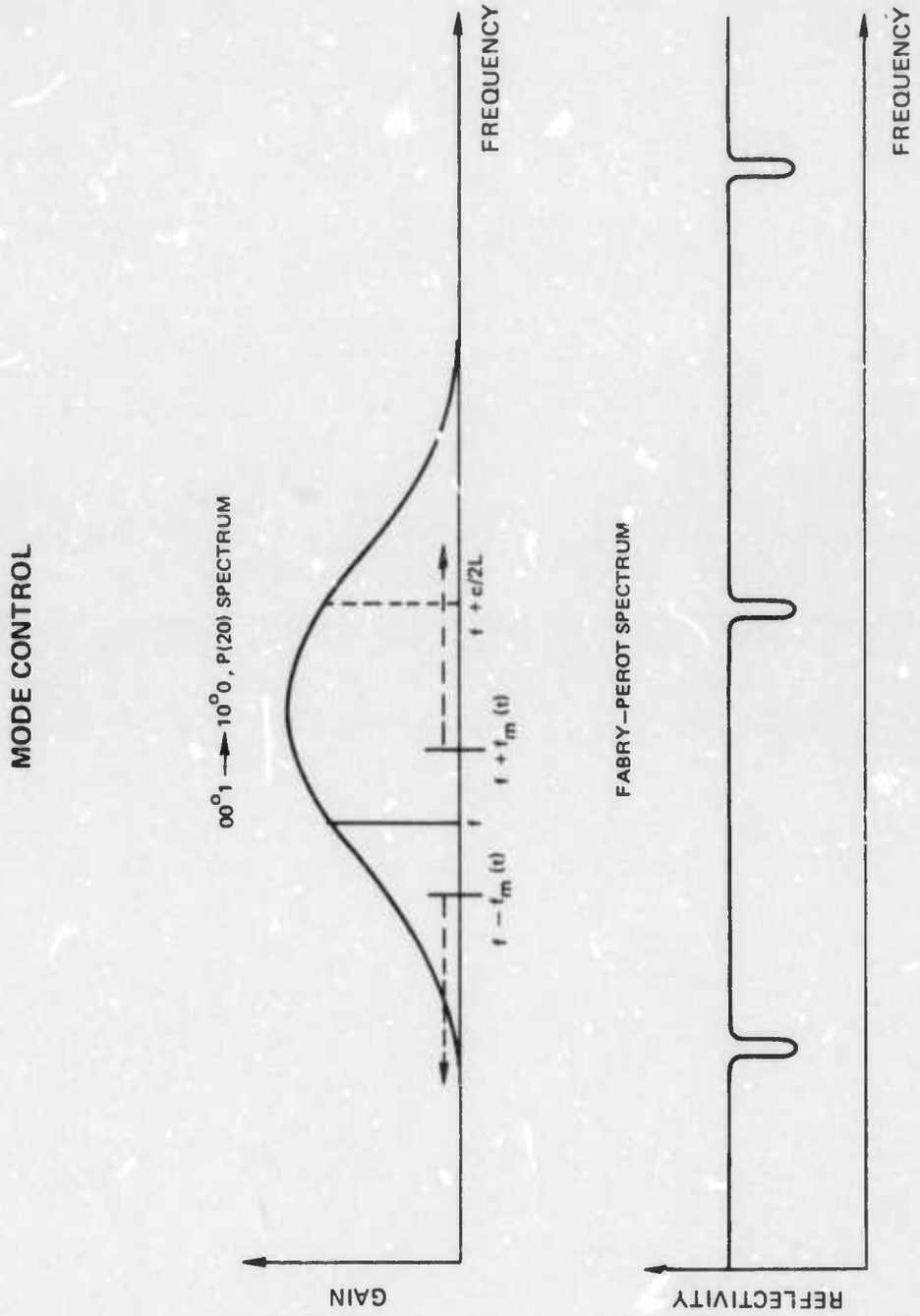
MODE CONTROL
$00^01 \rightarrow 10^00$, P(20) SPECTRUM
GAIN
FREQUENCY
$f + c/2L$
$f + f_m(t)$
f
$f - f_m(t)$
FABRY–PEROT SPECTRUM
REFLECTIVITY
FREQUENCY

A prime goal of our investigation is to determine the system's modulation response for a frequency sweep in excess of c/2L; i.e., a sweep of the optical frequency from the initial value through one neighboring suppressed axial resonance. It, therefore, suffices to consider a system where only two axial resonances fall inside the gain profile, as illustrated in Fig. 4. In that case, our mode selection technique is adequate.

Very high-pressure waveguide lasers, however, may have more than two axial modes inside the active spectral region (dependent on the minimum achievable resonator length); in which case, one must resort to a different mirror arrangement as for instance the one illustrated in Fig. 5 (Ref. 2).

To measure the modulation response, the output of the waveguide laser is heterodyned with a stable, fixed frequency, optical local oscillator in a wide-band photodetector; the resulting frequency-chirped rf signal is mixed with a second frequency-swept signal (sampled from the drive circuit) in an rf square law detector and the beat frequency (BF) fed into a spectrum analyzer (see Fig. 6). If the modulation response is linear, one observes a sharp sinusoidal signal at the rf mixer output. Deviations from the ideal sinusoid indicate modulation distortion.

Implementation of a frequency sweep from dc to 500 MHz calls for a wide-band match of the rf signal to the modulator. A simple matching circuit consists of a 50Ω load across the modulator electrodes at the end of a 50Ω line carrying the drive signal. It is shown in the following that a rf-power of more than 500 W is required to obtain 2 percent output coupling.

FIG. 5

IMPROVED MODE SELECTION

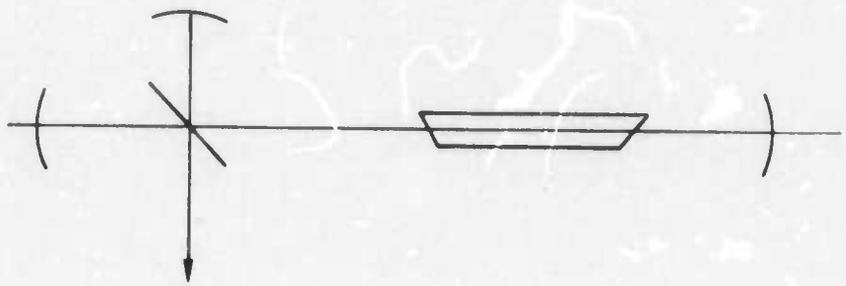

FIG. 6

DEMODULATION SYSTEM

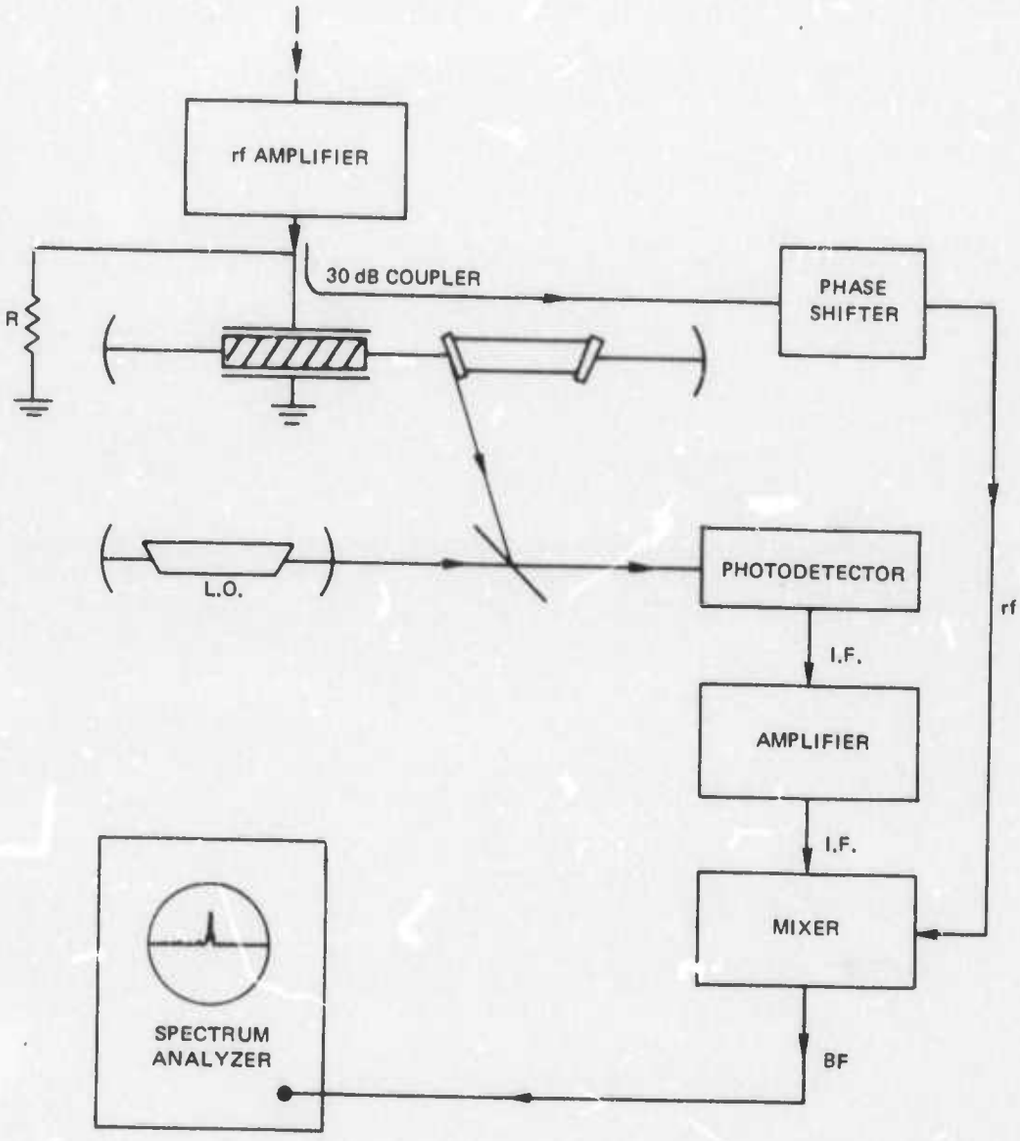

3.0 EXPERIMENTAL RESULTS

3.1 Waveguide Lasers

During the reporting period, we fabricated and tested flowing and sealed-off CO_2 waveguide lasers to determine the design most suitable to our investigation.

Photographs of open-cycle and sealed-off waveguide lasers are shown in Figs. 2 and 7, respectively. The use of a hollow dielectric (BeO) waveguide both to guide the laser light and to confine a gas discharge provides an optimum match between the optical wave and the active medium. For the CO_2:He:N_2 laser, as with many other gas lasers, narrowing the bore of the discharge tube results in increased gain, linewidth, power generated per unit volume and intensity saturation parameter. These benefits result from favorable de-excitation by wall collisions, operation at increased pressures and, in the case of the CO_2 system, from reduction of the gas temperature due to improved thermal conduction to the wall. The possibility of operating at high gas pressures results from the scaling properties of the tube-confined gas discharge plasmas. If the pressure is varied inversely as the tube diameter, the electron energy distribution remains constant (Ref. 3). One would then expect that electron collision excitation processes, which are dominant for this laser, would remain qualitatively unchanged. Higher pressures, however, give increased pressure-broadened linewidth and increased power generation per unit volume.

The optical beam inside a waveguide laser switches back and forth between free space and guided propagation. The light propagates through a capillary in form of the lowest order linearly polarized EH_{11} guided mode. After exiting the capillary, the laser radiation impinges on a concave mirror and is refocused back into the capillary. This transition between free space and guided propagation is 98 percent efficient. Thus, due to this excellent match between the EH_{11} waveguide mode and the lowest order free space eigenmode (TEM_{oo}), very little loss is incurred by the repeated change from free to guided propagation and back to a free propagation again (Ref. 4). It is worth noting that linearly polarized guided modes of higher order do not have a free space counterpart with such a good match and are, therefore, suppressed by the system. Consequently, the refocusing by the concave mirrors performs effective mode selection by suppressing all but the desired lowest order mode.

The steady state behavior of a low gain, homogeneously broadened laser is described by (Ref. 5)

$$2\, g\, \ell\, (1 + 2I_i/I_s)^{-1} = \alpha + T, \qquad (1)$$

where ℓ is the length of the plasma column, g the unsaturated exponential power gain coefficient per unit length of the active medium, I_i is the one-way power flow density inside the resonator, I_s is the saturation parameter (i.e., the power density for which the gain is saturated to -3 dB of the small signal value), α is the intracavity

FIG. 7

SEALED–OFF WAVEGUIDE LASER

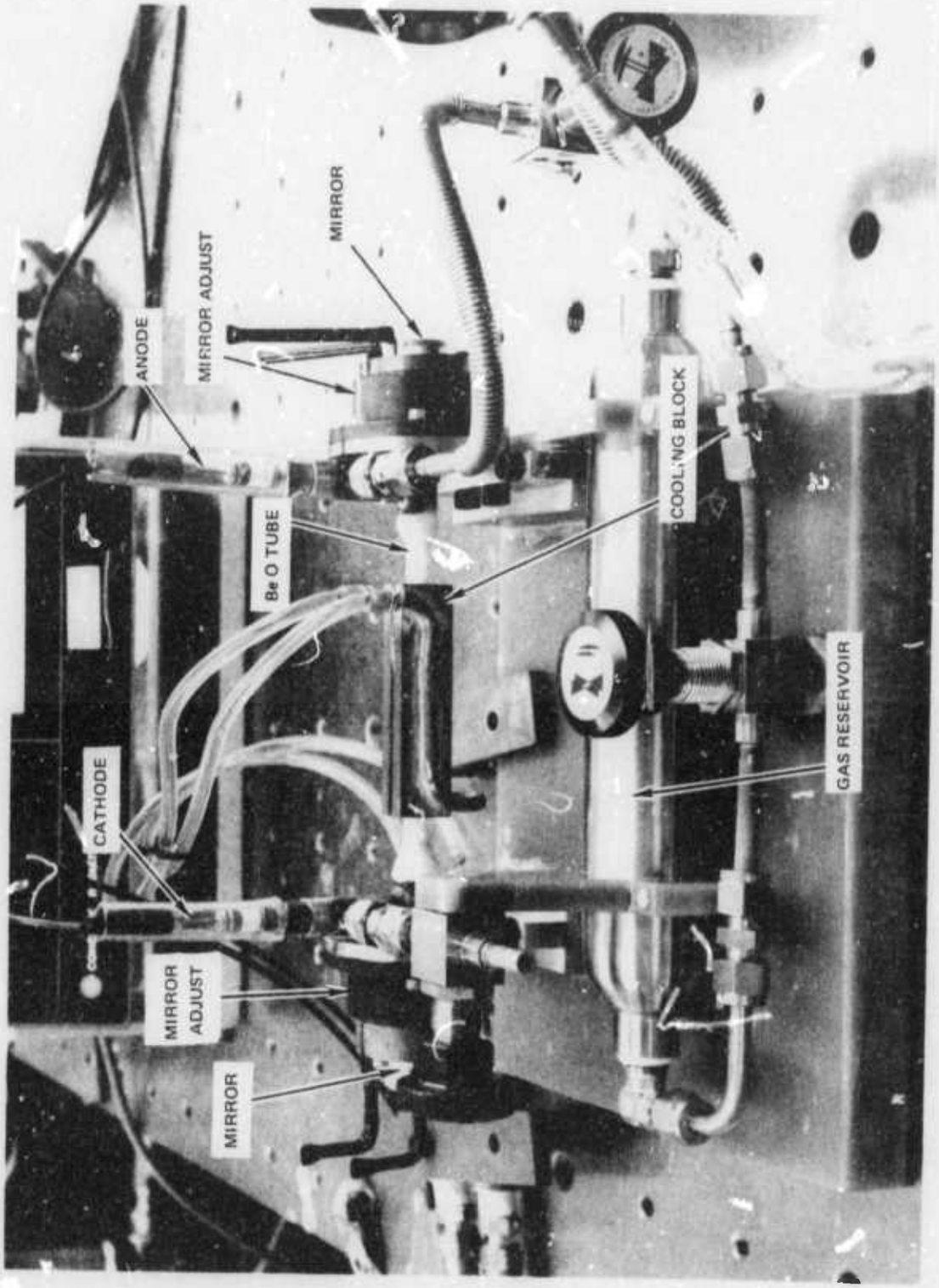

RL–73–204

loss encountered upon a round-trip transmission through the resonator and T is the relative transmission of the output mirror. Equation (1) states that the power saturated gain of the active medium has to compensate for the total optical loss consisting of output coupling and resonator losses (imperfect reflection at the mirrors, transition from free space to guided propagation, radiation leakage into the capillary wall, absorption in the modulator, and reflection off the modulator faces). The output power density is given by $I_o = T \times I_i$, hence

$$I_o = \tfrac{1}{2}T \cdot I_s [2g\ell/(\alpha + T) - 1]. \qquad (2)$$

It can be shown that for a given gain and loss coefficient, I_o is optimized if $T = \sqrt{2g\ell\alpha} - \alpha$. From Eq. (2) then follows for the maximum output power density

$$I_o = \tfrac{1}{2}I_s(\sqrt{2g\ell} - \sqrt{\alpha})^2. \qquad (3)$$

Equation (3) holds strictly for a beam of uniform intensity profile. For this case, the total power output is equal to I_o times the cross-sectional area of the beam. For the waveguide laser considered here, the surface area of interest is the capillary cross section. The intensity of the dominant waveguide mode (EH_{11}), however, is not of uniform distribution but has an axially symmetric profile which in the radial direction falls off as the lowest order Bessel function to a zero value at the waveguide wall. Assuming constant values of I_s, g and α across the beam, we obtain the output power by integration over the beam profile yielding

$$P_o = \tfrac{1}{2}\pi\sigma^2 I_s (\sqrt{2g\ell} - \sqrt{\alpha})^2, \qquad (4)$$

where σ is the e^{-1} radius of the intensity profile. The values for the gain and saturation parameters vary strongly with gas temperature and pressure but are typically substantially larger than for conventional large bore slow-flow CO_2 lasers, such that the power output per unit length of plasma is similar for both types of lasers (see Appendix D for a detailed discussion).

The CO_2 waveguide laser shown in Fig. 7 uses a water-cooled heat sink and has a 4.5 in. long active plasma length. This laser yields an output power of 1.5 W for a fill pressure of 100 torr. This preliminary laser was constructed for the purpose of investigating laser stability and lifetime and was not designed for optimum power output. By employing an improved cooling technique, replacing the concave reflectors with flat reflectors positioned close to the capillary and optimizing the output mirror transmission, we expect to double the output power to approximately 3 W.

3.2 Modulation Experiments

The modulation experiments were performed with a 1 mm diameter open-cycle system shown in Fig. 2 which used a 3:1:1 $He:N_2:CO_2$ mixture. For the 1 mm ID flowing system, optimum gas mixtures and discharge currents were determined for gas pressures ranging from 50 to 200 torr. It was found that a 3:1:1, $He:N_2:CO_2$ ratio is close to an optimum

mixture through this entire pressure range. The dependence of output power on discharge current is very flat at all pressure values between 50 and 200 torr. While higher currents provide a larger excitation rate into the upper laser level, 00^01, they also cause increased gas heating which enhances the population of the lower laser level, 10^00, due to an increased bottleneck at the 01^10 to 00^00 terminating transition. The compromise between these two conflicting processes determines the optimum discharge current, which rises from a value of approximately 2 mA at 50 torr to a value of 5 mA at 200 torr for the 1 mm ID 10 cm long BeO plasma tube. The total flow rate was varied from 10 cm^3/sec (standard pressure) at 50 torr to 40 cm^3/sec at 200 torr pressure. To remove the discharge heat the BeO tube was clamped to a water-cooled copper block.

Using a maximum reflection mirror of 25 cm radius of curvature and a 20 cm radius of curvature mirror with 5 percent transmission, it was found that the maximum output power was achieved if the center of curvature of each mirror was located about 1 cm inside the capillary. Under this condition we obtained an output power of 750 mW at 100 torr average pressure. When the modulating element was inserted into the resonator, a 50 percent power drop was observed

To restrict the laser oscillation to the P(20) line, we replaced the 25 cm mirror by a positive CdTe lens followed by a diffraction grating employed in Littrow alignment (Fig. 3). The lens was positioned approximately at the focal distance from the capillary opening such that the laser beam left the lens collimated and, after retro-reflection from the blazed grating, was refocused into the capillary. The laser output was monitored with an Optical Engineering Laser Spectrum Analyzer; stable P(20) oscillation was observed.

3.3 Modulator Design

An additional advantage of the waveguide design is the small beam diameter in the vicinity of the capillary opening, permitting the use of modulator elements with small cross section.

The change in optical length of the modulator element is given by

$$\Gamma_o = \pi \frac{V}{V_{\lambda/2}} , \tag{5}$$

where V is the applied peak voltage and $V_{\lambda/2}$ is the voltage required to obtain a phase shift of one-half wavelength defined by the expression (Ref. 6)

$$V_{\lambda/2} = \frac{\lambda h}{2(n_o)^3 r_{41} \ell} , \tag{6}$$

where λ is the optical wavelength; n and r_{41} are the index of refraction and the relevant electro-optic constant, respectively, for CdTe, cut and oriented for maximum AM-modulation; h the height of the crystal in the direction of the applied field; and ℓ the length of the modulator crystal. For the modulation band considered here, dc - 500 MHz, efficient coupling of the rf power to the capacitive modulator element is best obtained by connecting a shunt resistance R in parallel to the electrodes of the modulator such that the total impedance is approximately equal to R.

From Eq. (A5), Appendix A, follows that the instantaneous power in the coupled, cross polarized, sidebands is $P = \eta P_i \sin^2 \Gamma$; where η is the coupling efficiency, given by the relative reflection off the Brewster plate; P_i the internal one-way power; and $\Gamma = \Gamma_o \sin \omega_m t$. Note, that a double pass through the modulator is taken into consideration. For $\Gamma \ll 1$ we obtain the average output power of

$$\bar{P}_{out} = \eta \cdot P_i \frac{1}{2} \left(\frac{V \cdot \pi}{V_{\lambda/2}} \right)^2 . \tag{7}$$

Solving for the peak rf voltage we get

$$V = \left(\frac{2 \bar{P}_{out}}{\eta P_i} \right)^{\frac{1}{2}} \cdot \frac{V_{\lambda/2}}{\pi} , \tag{8}$$

which requires an average rf-power of

$$\bar{P}_{rf} = \frac{1}{2} \frac{V^2}{R} = \frac{\bar{P}_{out}}{\eta P_i R} \left(\frac{V_{\lambda/2}}{\pi} \right)^2 . \tag{9}$$

Substituting the values $\eta = 0.5$; $P_i = 5$ W; $V_{\lambda/2} = 2.7$ kV (Ref. 7) (for d = 0.2 cm and $\ell = 4.0$ cm); and R = 50Ω, we get

$$\bar{P}_{rf} = \bar{P}_{out} \cdot \frac{(2.7)^2 \times 10^6}{(0.5) \times 5 \times 50 \times \pi^2} = \bar{P}_{out} \cdot (5.8) 10^3 . \tag{10}$$

Thus, to obtain $P_{out} = 0.1$ W we require an rf power of 580 W. The presently employed modulator crystal is 0.3 cm wide. It was found during the experiment, however, that a crystal width of 0.2 cm does not lead to any noticeable beam vignetting; consequently, it is possible to use such a narrow modulator. While there is no principle problem in attaining a 500 W amplifier for the bandwidth of interest, the purchase of such a costly, specially designed, device is not within the means of this contract and not necessary in order to prove the viability of the here investigated modulation format. Presently, we employ a 2 MHz - 500 MHz broadband amplifier yielding 1/3 W into a 50Ω matched load. High-power modulation would belong to a future phase of this development.

3.4 Fixed Frequency Modulation

The first test of the modulated waveguide laser was conducted at a fixed frequency of 2 MHz. Figure 8 shows the demodulated signal in time and spectral display. The photographs on the left side represent the ideal case in which the demodulated signal consists of a sinus function at frequency $2f_m$ (the beat note between the two sidebands), indicating complete suppression of the carrier frequency. The photographs on the right side show a case in which, aside from the sidebands, part of the carrier is coupled from the resonator such that the demodulated signal contains spectral components at f_m as well as $2f_m$. The f_m-component results from mixing of the sidebands with the "leaked" carrier component, while the $2f_m$-component is the beat note between the two sidebands. Note that the time display in the second case also shows the presence of the f_m-component in that every second maximum is enhanced.

The second condition is undesirable since it compromises the isolation of the selected sideband. Carrier leakage is caused: (1) by a misalignment of modulator crystal and Brewster window; and (2) by stress birefringence inside the modulator or the Brewster plates of the plasma tube. While alignment between the modulator (001) axis and the plane of incidence for the Brewster plates can be accurately controlled, the effect of stress birefringence is more difficult to overcome. Carrier suppression was obtained by mirror adjustment, which suggests that the position of the optical axis was varied until a beam path was found which minimized the depolarization.

3.5 Chirp Modulation

Employing the above described laser, we obtained a frequency-chirped optical signal by applying the output of a H-P 8690 Sweep Oscillator, after amplification, to the electrodes of the CdTe modulator. The sweep range was varied up to the full band of 2 MHz to 500 MHz and the coupled optical signal was demodulated by a Ge:Hg photoconductor. The base-band signal, after appropriate amplification, was displayed on a HP 8155 Spectrum Analyzer. Figure 9 shows the demodulated signal for a 2 to 100 MHz sweep.

In order to obtain a dense display of the spectrum on the oscillograph screen, the sweep speed was reduced to a low value (1 sec full range) dictated by the sampling speed of the analyzer. The demodulated output signal shows variation in amplitude which repeats itself on subsequent spatial displays taken during the experiment. At present, the cause for this fluctuation is not well understood; indications are that it relates to a variation in the load impedance with frequency. When the sweep range was increased to 2-500 MHz, the fluctuations in the spectrum increased even more. Above 250 MHz, a fraction of the drive voltage at f_m was picked up by the detector circuit. For the large sweep range it became apparent that the load impedance exhibited large variation with frequency because the simple circuit described above is significantly modified by stray capacitances and inductances of the device. It was found; for instance, that at 400 MHz the signal was almost totally reflected from the load; simultaneously, a strong pick-up signal was observed as might be expected since the reflected signal interferes with the incident one to form a large standing wave.

FIG. 8

FIXED FREQUENC ' MODULATION

rf SPECTRUM

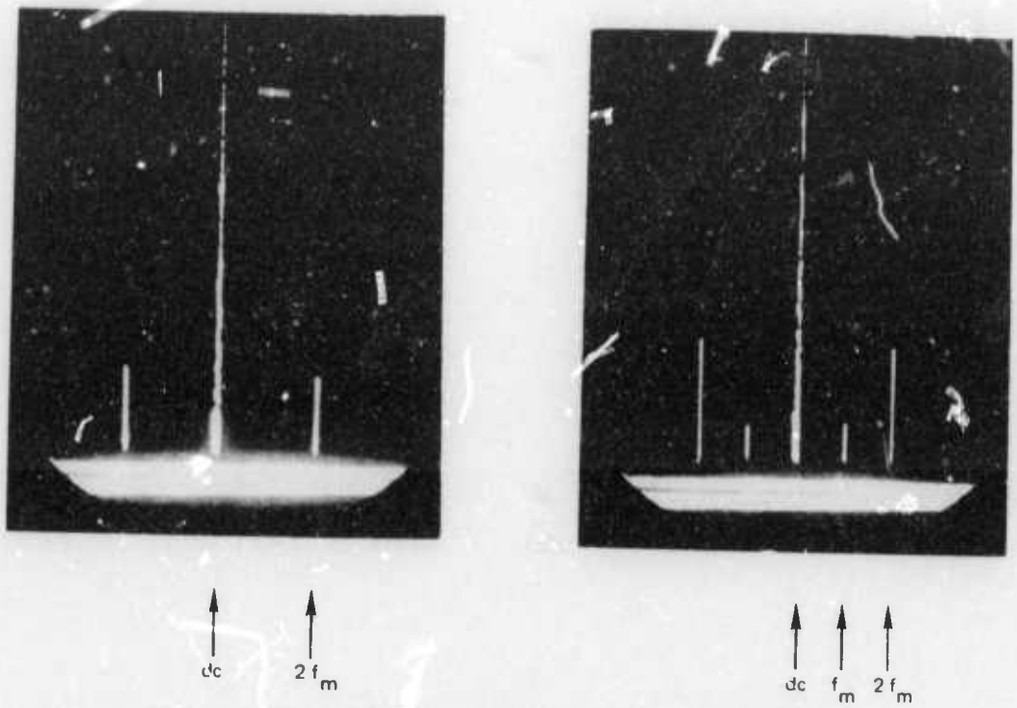

SIGNAL VOLTAGE VS TIME

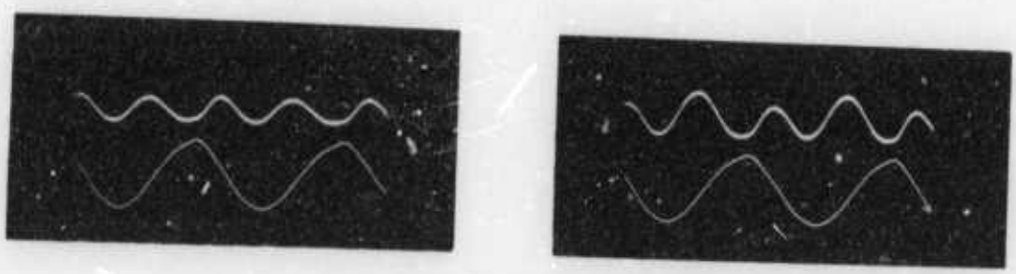

UPPER TRACE: DEMODULATED SIGNAL
LOWER TRACE: MODULATING SIGNAL

FIG. 9

CHIRPED SIGNAL

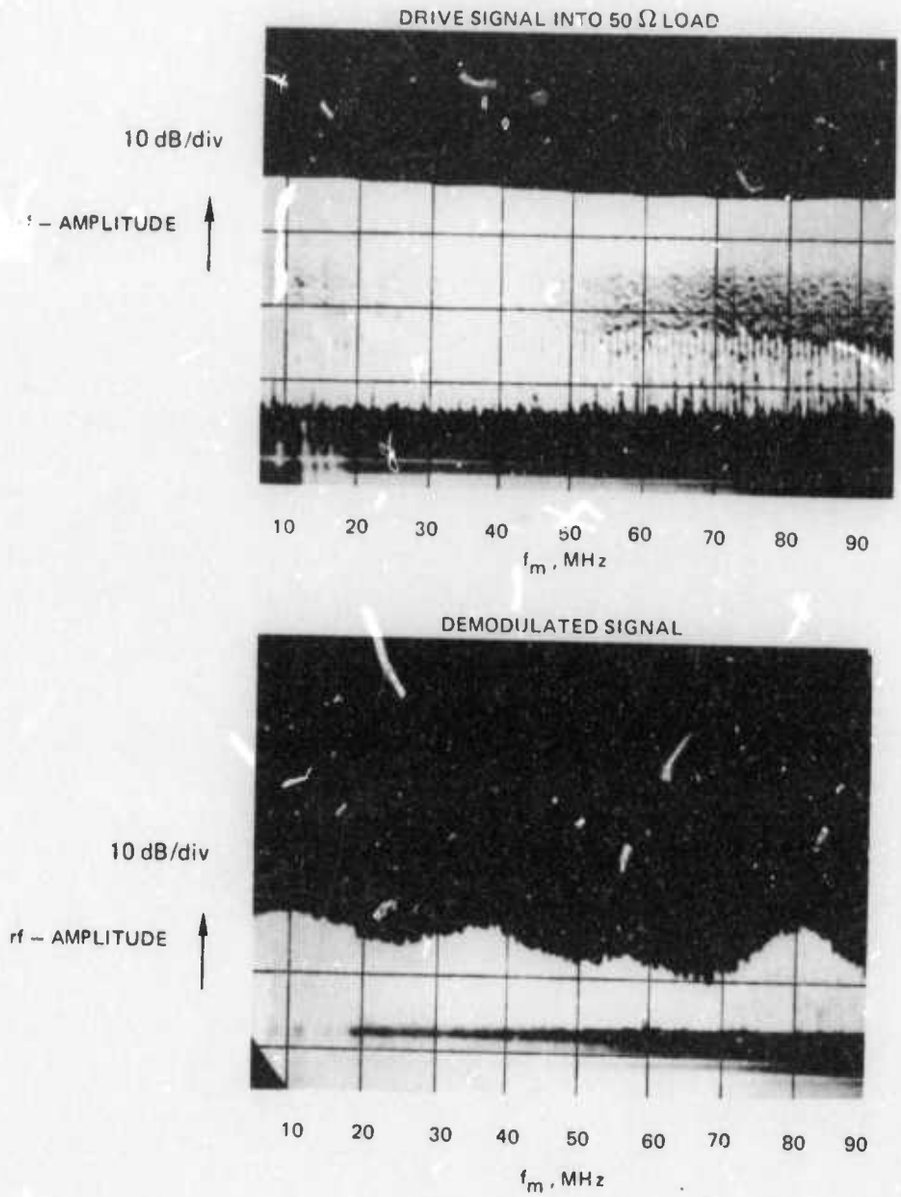

It is useful to recall the essential feature of our matching technique; namely, the use of a resistive element parallel to the electrode surfaces of the modulator. The total circuit then assumes the form shown in Fig. 10a where the dominant elements are the modulator capacitance C and the shunt resistance R. Stray capacitances and inductances are present due to the wires connecting the electrode surfaces with the 50Ω cable. The input impedance Z_{in} given by the expression

$$Z_{in} = \frac{1/R - i\,1/X}{(1/R)^2 + (1/X)^2} \qquad (11)$$

where $X = \omega(L - 1/C)$. If R is sufficiently small compared to X, $Z_{in} \approx R$. As the frequency increases beyond a critical value, X becomes larger than R and the reflectivity varies with ω. For the work reported here, the value of R was chosen to equal 50Ω to obtain a good match to the power amplifier impedance. The experiment, however, showed that in order to dominat the impedance up to values of 500 MHz, R must be considerably smaller than 50Ω.

An impedance step-down could be accomplished by a commercially available rf transformer but at the cost of reducing the plate voltage with the impedance. To obtain an impedance step-down while simultaneously retaining the rf supply voltage across the modulator, an active matching circuit must be employed. For the impedance values of interest, it is convenient to use a power rf-transistor in common-collector mode of operation (also called an emitter follower) which is equivalent to the familiar cathode follower tube circuit (see Fig. 10b). An emitter follower matching circuit with a step-down of 4:1 is presently under construction at UARL. It should be adequate to provide a flat impedance from 2 MHz to 500 MHz. Furthermore, to minimize stray capacitance and inductance, the modulator will be mounted in close proximity to the transmitter as shown in Fig. 11 where the CdTe crystal is placed directly on the PC board carrying the transistor and the resistive shunt.

3.6 Modulation Response at c/2L

As stated previously, one of the main goals of this program is to investigate the modulation response of the system in the presence of mode selection. It should be recalled that mode selection is necessary to assure the presence of only <u>one</u> carrier frequency. Since the signal sidebands sweep through a range exceeding intermode spacing, one must be concerned with the response of the system as the sideband of interest sweeps through suppressed cavity resonances. Although prevented from self-oscillation by the mode selection, it is nevertheless possible that at the moment of synchronism betweeen the modulating, f_m, (or its harmonic $2f_m$) and the intermodal frequency, c/2L, sufficient power is coupled into the suppressed resonance to initiate a damped oscillation at that mode. The spurious oscillation of such unwanted modes is then also modulated, creating a second set of chirped sidebands about the carrier frequency f_o + c/2L, which after demodulation, add to the main chirped signals but with different phase and with temporally decaying amplitude. The result would be a distortion of the main chirp signal.

FIG. 10

MATCHING CIRCUITS

a) PASSIVE NETWORK

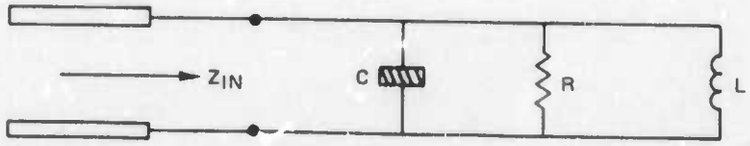

b) EMITTER–FOLLOWER

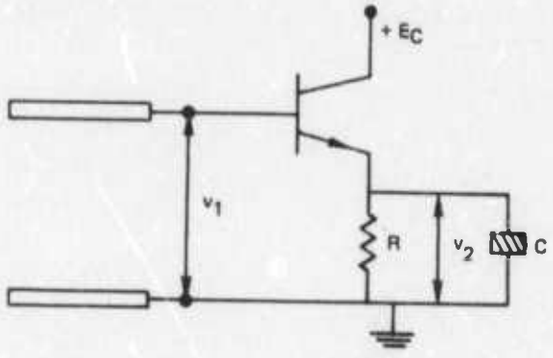

FIG. 11

EMITTER FOLLOWER

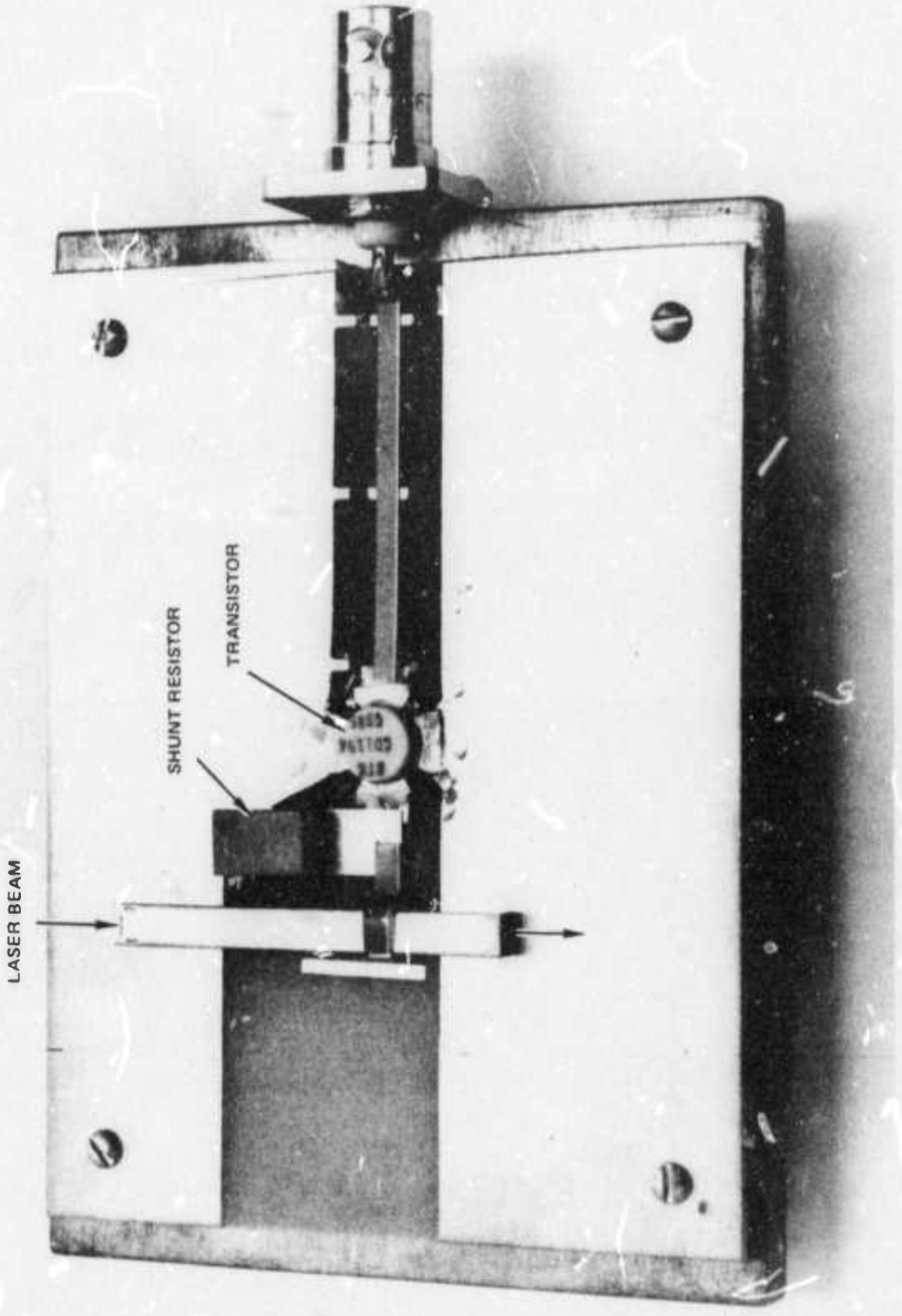

RL 73--286

An illustration of resonant behavior is shown in Fig. 12 which was obtained with the above system (no mode selection present) when the modulation frequency f_m was slowly tuned into synchronism with c/2L. The pulses shown in Fig. 12 result from a coherent summation of demodulated signals at the frequencies c/2L, 2c/2L, 3c/2L, etc.; i.e., the resonant modulation forced oscillation of several optical modes with fixed phase relations among them such that the sum of their difference frequencies add up coherently to yield the displayed pulses; in short, the system was mode locked. Viewing the demodulated signal on a spectrum analyzer screen, a concomitant enhancement of the demodulated signal at c/2L was observed. Two questions arise: (1) will there be such resonant behavior in the presence of mode selection; and (2) does the resonance response change for very fast frequency sweeps when the time period during which the drive signal is inside the locking range is shorter than the cavity round-trip time. These problems will be addressed by the experiments planned for the next reporting period.

FIG. 12

MODELOCKED SIGNAL

UPPER TRACE: 114 MHz MODULATION SIGNAL

LOWER TRACE: DEMODULATED OPTICAL SIGNAL

(WIDTH BETWEEN HALF–POWER POINTS OF PULSES IS 2.8 nsec)

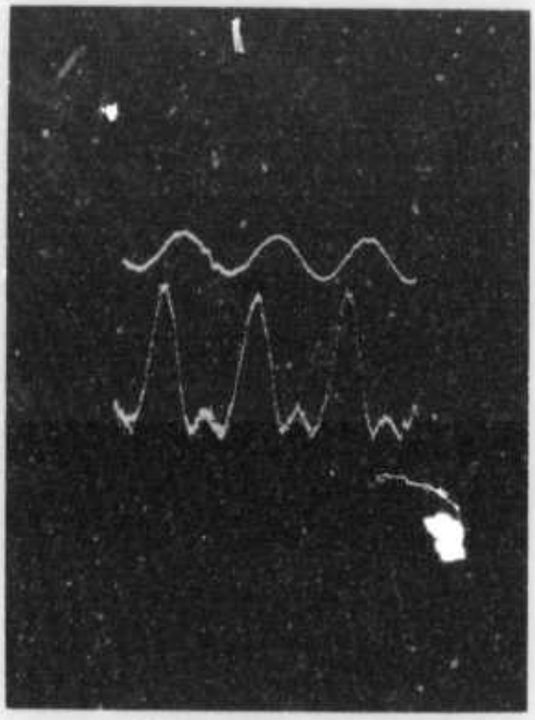

10 nsec

4.0 DISCUSSION AND FUTURE PLANS

During this reporting period linear FM-modulation was obtained for a CO_2 waveguide laser by employing coupling modulation and sweeping the modulator frequency in linear fashion. This represents an important step towards the contract goal to obtain fast chirp modulation, such that the instantaneous frequency starts from a spectral position in the wing of the P(20) gain profile and sweeps over a range which exceeds one axial mode spacing c/2L.

The original waveguide laser was modified by replacing one mirror with a Fabry-Perot system comprised of a Littrow diffraction grating and a semitransparent mirror such as to selectively reduce the optical reflectivity for all but the P(20) line and within that line for certain narrow spectral ranges. In our experiment we select gain bandwidth and axial mode spacing and position such that two modes of the large cavity fall within the line. They are placed symmetrically about line center and one mode is suppressed by adjusting the spacing of the auxiliary Fabry-Perot such that one of its reflection minima coincides with that mode (see Fig. 4).

Modification of the waveguide laser to accomplish the above mode control has been completed and testing of the new system is under way. The next step involves an experimental setup as shown in Fig. 6, where the chirp signal is first heterodyned with an optical local oscillator, the demodulated chirp signal is then mixed with a split-off portion of the driving rf-signal and the beat frequency, BF, is observed with a spectrum analyzer.

For the ideal signal, the spectrum analyzer displays a single constant frequency. Carrier fluctuation and modulation distortion (for instance, due to resonant response at the c/2L modulation frequency) will be reflected by a widening of the beat frequency.

In order to obtain constant rf-coupling into the modulator device over the full 500 MHz chirp range, we designed an active matching circuit consisting of an emitter follower to transform the 50Ω source impedance to a 12.5Ω shunt resistor connected across the modulator electrodes.

A second task performed during the reporting period is the design, manufacture, and testing of a sealed-off CO_2 waveguide laser (important to the program for the frequency stability achievable with sealed-off lasers). Bore diameter, fill pressure and gas composition were varied to optimize the performance of the device. A maximum output of 1.5 W was achieved for a 1.5 mm ID, 12.5 cm long BeO plasma tube at 20°C filled to 100 torr gas pressure with a mixture of $He:N_2:CO_2:Xe:H_2$ in the ratio of 4:1:1:0.13:0.1.

5.0 REFERENCES

1. T. Gilmartin, Lincoln Laboratory: private communication.
2. P. W. Smith: "On the Stabilization of a High-Power Single-Frequency Laser," IEEE J. Quan. Elec. QE-2, 666 (1966).
3. D. D. Cobine: "Gaseous Conductors," Dover, New York (1958).
4. R. C. Abrams and A. N. Chester: Opt. Soc. of America Spring Meeting, Denver, Colorado (March 1973).
5. J. E. Geusic, et. al.: "Continuous 0.532μ Solid-State Source Using $Ba_2NaNb_5O_{15}$," Appl. Phys. Lett. 12, 306 (1968).
6. I. P. Kaminow and E. H. Turner: Proc. of the IEEE 54, 1374 (1966).
7. D. E. Kiefer, et. al.: "Intracavity CdTe Modulators for CO_2 Lasers," IEEE J. Quan. Elec. QE-8, 173 (1972).

APPENDIX A

AM TECHNIQUES

Amplitude modulation is employed to generate sidebands which are then chirped by sweeping the modulating frequency. To obtain the required chirped signal, one sideband must be isolated from the optical signal. AM modulation can be obtained either by intracavity or external AM modulation. Electro-optical amplitude modulation generally operates on the principle of modulating the state of polarization of the optical wave such that part of the optical power is coupled from the dominant polarization to the orthogonal one. Both are then amplitude modulated. External modulation suffers from inefficiency since the sideband of interest contains only a small fraction of the incident light whereas most of the optical power is lost. By placing the modulator inside the resonator, one can retain the dominant polarization component inside the resonator while coupling only the orthogonal component from the cavity (coupling modulation). The figure below shows the index ellipse associated with the electro-optic effect employed in the case discussed here (Ref. 6). The incident field, polarized parallel to $\bar{a}_{||}$

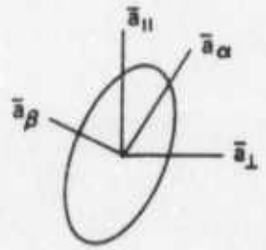

can be expressed in components of the principal vectors $\bar{a}_{\alpha}$ and $\bar{a}_{\beta}$

$$E_{\alpha} = 1/\sqrt{2}\ E_o\ e^{i(kr-\omega_o t)} \tag{A1}$$

$$E_{\beta} = 1/\sqrt{2}\ E_o\ e^{i(kr-\omega_o t)}. \tag{A2}$$

Upon propagation through the crystal, one principal component exhibits a phase lag, the other a phase advance of equal value;

$$E'_{\alpha} = 1/\sqrt{2}\ E_o\ e^{i(kr-\omega_o t+\frac{1}{2}\Gamma)} \tag{A3}$$

$$E'_{\beta} = 1/\sqrt{2}\ E_o\ e^{i(kr-\omega_o t-\frac{1}{2}\Gamma)}. \tag{A4}$$

Expressing the fields now again in the original coordinate system ($\bar{a}_{||}$, $\bar{a}_{\perp}$) we find

$$E_{\perp} = 1/\sqrt{2}\ (E_{\alpha} - E_{\beta}) = i\, E_o \sin \tfrac{1}{2}\Gamma\, e^{i(kr-\omega_o t)} \quad (A5)$$

$$E_{\parallel} = 1/\sqrt{2}\ (E_{\alpha} + E_{\beta}) = E_o \cos \tfrac{1}{2}\Gamma\, e^{i(kr-\omega_o t)}. \quad (A6)$$

Suppressing the common spatial term and substituting $\Gamma = \Gamma_o \cos \omega_m t$, we get

$$e_{\parallel} = (1 - \tfrac{1}{16}\Gamma_o^2) \cos \omega_o t - \tfrac{1}{32}\Gamma_o^2 \{\cos (\omega_o + 2\omega_m)t + \cos (\omega_o - 2\omega_m)t\}, \quad (A7)$$

$$e_{\perp} = \tfrac{1}{4}\Gamma_o \{\sin (\omega_o - \omega_m)t - \sin (\omega_o + \omega_m)t\}. \quad (A8)$$

Similarly, if the modulating signal is augmented by a bias voltage, such that $\Gamma = \gamma + \Gamma_o \cos \omega_m t$, we obtain for the two principal polarization components

$$e_{\parallel} = (1 - \tfrac{1}{8}\gamma^2 - \tfrac{1}{16}\Gamma_o^2) \cos \omega_o t - \tfrac{1}{8}\gamma\Gamma_o \{\cos (\omega_o + \omega_m)t + \cos (\omega_o - \omega_m)t\}$$
$$- \tfrac{1}{32}\Gamma_o^2 \{\cos (\omega_o + 2\omega_m)5 + \cos (\omega_o - 2\omega_m)t\}, \quad (A9)$$

$$e_{\perp} = \tfrac{1}{2}\gamma \sin \omega_o t + \tfrac{1}{4}\Gamma_o \{\sin (\omega_o + \omega_m)t + \sin (\omega_o - \omega_m)t\}. \quad (A10)$$

A comparison of the two cases shows that the biased system yields carrier and second order sidebands in the dominant polarization and first order sidebands-suppressed carrier in the orthogonal polarization. For the biased modulator, both polarizations contain carrier and first order sidebands, while the dominant polarization also possesses second order sidebands.

The increase in modulation efficiency relates to the fact that the optical power inside the laser resonator is larger than the external power by a factor F, equal to the finesse of the cavity, which for the "empty" resonator, is of the order of 100 if neither end mirror is used to couple out power. With the insertion of the modulator, however, the finesse is reduced to $F \approx 10$.

The advantage of extracavity modulation is that ultrastable operation has been achieved by purely passive means; i.e., control of power supply ripple and reduction of mechanical vibration and drift. Insertion of a modulator into the optical cavity leads to frequency drift due to heating of the electro-optic crystal and a concomitant change in its optical length. A second source of instability relates to distortion of the AM signal (FMing) brought on by misalignment of the electro-optic geometry. While the thermal drift may be reduced by operating the modulator at constant rf input power and in cw fashion, the FMing can be eliminated by accurate electro-optic alignment; the question remains whether fluctuation of the crystal temperature and FMing can be sufficiently repressed to obtain the desired carrier stability.

Another problem associated with coupling modulation relates to the existence of axial resonances spaced at the intermodal frequency c/2L. While the bandwidth of coupling modulation is not limited by the gain profile, or the intermodal frequency,

an anomalous response can generally be expected at the moment in which the modulator frequency, f_m, is in synchronism with the intermodal frequency c/2L. In fact, if the modulation frequency is slowly tuned into synchronism with the intermodal frequency, mode locking takes place, which distorts the sinusoidal AM signal into a series of sharp repetitive pulses spaced at 2L/c. There are two questions to be answered: (1) will there be such resonant behavior if all but one axial mode are strongly suppressed by appropriate mode selection and (2) does the resonance response change for fast frequency sweeps where the time period during which the drive signal is inside the locking range is shorter than the cavity round-trip time.

Finally, it should be noted that both AM techniques require that the chosen sideband be isolated from the total optical signal. This can be accomplished; for instance, by placing the carrier on a different molecular transition, such as a line from another CO_2 isotope, at a spectral distance of f_a from the conventional P(20) line. The center frequency of the frequency-chirped modulation signal is then chosen to equal f_a such that one AM sideband sweeps about the P(20) center frequency as desired. This, in effect, separates the selected sideband from the total optical signal in that only that sideband falls inside the gain profile of the radar transmitter's laser amplifiers at P(20).

Carrier off-set from P(20) line center may also be obtained if a wide-band laser, such as a waveguide system at P(20), is used and one active resonance is singled out by mode selection and tuned to the side of the gain profile. The main attractive feature of AM modulation external or internal, then, is the potential to obtain several gigahertz of bandwidth, since (for the case of carrier off-set via the use of isotope transitions), the bandwidth is limited only by the performance of the rf sweep generator and amplifier and the response of the modulator device.

APPENDIX B

TOLERANCE OF E-O ALIGNMENT

By electro-optical (E-O) alignment we mean the relative orientation of crystal axes, applied field, optical propagation direction and optical polarization. A sketch indicating the nominal alignment of our modulator is shown below. The beam

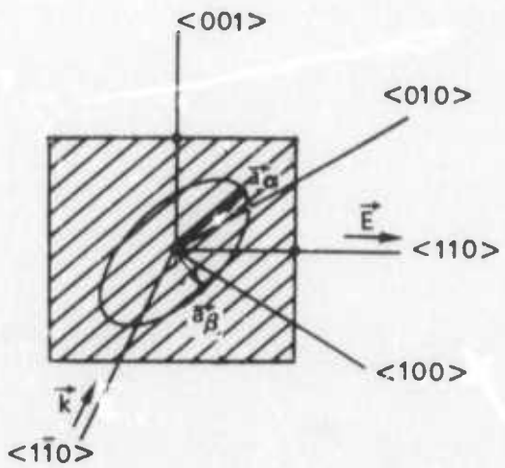

propagates along the ($1\bar{1}0$) direction and the applied electric field is along (110). The electro-optic effect is represented by the index ellipse shown in the shaded plane. Note that the principal axes, $\vec{a}_\alpha$ and $\vec{a}_\beta$, bisect the (001) and (110) lines. If the optical polarization of a beam of unit field strength is along the (001) or (110) direction, the incident field has equal components along the principal axes.

Let us assume that the polarization is parallel to the (001) direction. The beam emerging from the crystal consists then of the two principal components;

$$E_\alpha = 1/\sqrt{2}\ e^{i(kr-\omega_o t+\frac{1}{2}\Gamma)} \tag{B1}$$

$$E_\beta = 1/\sqrt{2}\ e^{i(kr-\omega_o t-\frac{1}{2}\Gamma)}, \tag{B2}$$

where k is the wave vector component along the propagation direction, r the coordinate along the propagation direction, $\omega = 2\pi$ the optical frequency, and $\pm \frac{1}{2}\Gamma$ the phase advance and retardation, respectively, of the principal field components and

$$\Gamma = 2\pi/\lambda \cdot \ell \cdot n_o^3\, r_{41}\, E_o \cos \omega_m t, \tag{B3}$$

where ℓ is the crystal length, λ the optical wavelength, n_o the intrinsic index of refraction of the crystal, r_{41} the relevant electro-optic coefficient, E_o the peak voltage of the applied field, and $\omega_m/2\pi$ the modulation frequency. The field may be expressed in components parallel and orthogonal to the incident polarization direction,

$$E_{\parallel} = \cos \tfrac{1}{2}\Gamma \, e^{i(kr-\omega_o t)} \tag{B4}$$

$$E_{\perp} = i \sin \tfrac{1}{2}\Gamma \, e^{i(kr-\omega_o t)}. \tag{B5}$$

Note that both field components are <u>purely</u> amplitude modulated; no FM-distortion is present. The actual geometry in practical devices deviates slightly from the nominal one, owing to the tolerance in crystal orientation and optical and mechanical alignment.

We now consider the case where the (001) alignment is off in elevation by γ and in azimuth by δ, both very small angles. Defining cartesian coordinates x,y,z parallel to the crystal axes (001), (010) and (001), respectively, one can express the electro-optic effect for the CdTe crystal via a quadratic form defining the indicatrix,

$$(x^2 + y^2 + z^2) \frac{1}{n_o^2} + 2r_{41} (y \cdot z \cdot E_x + x \cdot z \cdot E_y + x \cdot y \cdot E_z) = 1, \tag{B6}$$

where $E_x = E \cos (45^o+\delta) \cos \gamma$, $E_y = E \sin (45^o+\delta) \sin \gamma$ and $E_z = E \sin \gamma$. Since $\delta, \gamma \ll 1$, one can approximate

$$E_x = E_y = 1/\sqrt{2}\, E, \; E_z = \gamma E. \tag{B7}$$

To obtain the desired index ellipse, we insert Eq. (B7) into (B6) and rotate the coordinates by 45 deg about the z-axis into the coordinate system x',y',z', such that the new x'-axis is parallel to the optical beam. By setting $x' = 0$, we get the following approximated expression for the index ellipse:

$$(y')^2(\frac{1}{n_o^2} + r_{41} \gamma E) + (z')^2 \frac{1}{n_o^2} + 2r_{41} y'z'E = 1. \tag{B8}$$

We note that the misalignment rendered the indicatrix unsymmetric in the coordinates. Upon diagonalization we find for the principal indices

$$n_\alpha = n_o + \tfrac{1}{2} n_o^3 r_{41} (1 - \tfrac{1}{2}\gamma) E \tag{B9}$$

$$n_\beta = n_o - \tfrac{1}{2} n_o^3 r_{41} (1 + \tfrac{1}{2}\gamma) E. \tag{B10}$$

It can be shown that Eqs. (B4) and (B5) now assume the form

$$E_{\parallel} = \cos \tfrac{1}{2}\Gamma \cdot e^{-i\epsilon}\, e^{i(kr-\omega_o t)}, \tag{B11}$$

$$E_{\perp} = i \sin \tfrac{1}{2}\Gamma \cdot e^{-i\epsilon}\, e^{i(kr-\omega_o t)}, \tag{B12}$$

where

$$\epsilon = \tfrac{1}{4}\Gamma_o \gamma(\cos \omega_m t + \varphi_m), \tag{B13}$$

$\omega_m/2\pi$ is the frequency of the applied field, and φ_m an arbitrary epoch angle.

Suppressing the spatial phase term e^{ikr}, we obtain from Eq. (B12) the real field component of the coupled beam:

$$\hat{E}_{\perp} = \sin [\tfrac{1}{2}\Gamma_o \cos (\omega_m t + \varphi_m)] \cdot \sin [\omega_o t + \epsilon_o \cos (\omega_m t + \varphi_m)], \tag{B14}$$

which shows the familiar form of frequency modulation as well as the desired amplitude modulation. Without loss of generality, we may set $\varphi_m = \pi/2$. Taking into consideration that $\Gamma_o \ll 1$ and that the beam makes a double pass through the crystal, we can develop Eq. (B14) into the form

$$\hat{E}_{\perp} = \Gamma_o \sin \omega_m t \{J_o(2\epsilon_o) \sin \omega_o t + J_1(2\epsilon_o) [\sin (\omega_o + \omega_m)t - \sin (\omega_o - \omega_m)t]$$

$$+ J_2(2\epsilon_o) [\sin (\omega_o + 2\omega_m)t - \sin (\omega_o - 2\omega_m)t] + \ldots\}. \tag{B15}$$

For $\epsilon_o \ll 1$, the Bessel terms are approximated by $J_o(2\epsilon_o) = 1$, $J_1(2\epsilon_o) = \epsilon_o$, $J_2(2\epsilon_o) = \epsilon_o^2$, etc.

Crystal orientation is usually accurate within 1.0 deg ($\gamma = 1.75\ 10^{-2}$ rad). For the value $\Gamma_o = 0.28$ (corresponding to 2 percent output coupling) we find $\epsilon_o = 1.2 \times 10^{-3}$, a very small FM distortion indeed.

Next, let us consider an optical misalignment where the incident polarization differs by a small angle from the nominal orientation; i.e., the incident field vector forms an angle $45^o + \beta$ with the major indicatrix axis, such that the separation into principle components is unsymmetric;

$$E_{\alpha} = 1/\sqrt{2}\ (1 - \beta), \tag{B16}$$

$$E_{\beta} = 1/\sqrt{2}\ (1 + \beta), \tag{B17}$$

and the emerging field components parallel and orthogonal to the incident polarization are:

$$E_{\parallel} = [\cos \tfrac{1}{2}\Gamma - i\,\beta \sin \tfrac{1}{2}\Gamma]\, e^{i(kr-\omega_o t)} \tag{B18}$$

$$E_{\perp} = [i \sin \tfrac{1}{2}\Gamma - \beta \cos \tfrac{1}{2}\Gamma]\, e^{i(kr-\omega_o t)}. \tag{B19}$$

Substituting $\Gamma = \Gamma_o \cos \omega_m t$, $\Gamma_o \ll 1$, and suppressing the spatial phase term, we obtain for the coupled component the approximate expression

$$\hat{E}_\perp = \tfrac{1}{4}\Gamma_o \{\sin (\omega_o - \omega_m)t - \sin (\omega_o + \omega_m)t\}$$

$$- \beta(1 - \frac{1}{16}\Gamma_o^2) \cos \omega_o t + \beta \frac{1}{32}\Gamma_o^2 \{\cos (\omega_o + 2\omega_m)t + \cos (\omega_o - 2\omega_m)t\}, \quad \text{(B20)}$$

which contains aside from the desired sidebands at $\omega_o \pm \omega_m$, a fraction of the carrier component and sidebands at $\omega_o \pm 2\omega_m$.

In summary then, misalignment of the crystal axes relative to the electric field results in FM-distortion whereas a deviation from the correct polarization angle causes leakage of carrier and second order sideband components into the coupled beam. Both modulation distortions, however, are very small for the cases of interest.

APPENDIX C

MODULATOR HEATING

Heating of the CdTe modulator crystal results (a) from absorption of the optical beam; and (b) from ohmic losses of the rf-signal. Accurate measurements on the optical absorption of the CdTe material yielded an absorption coefficient of less than 0.2 percent per centimeter. Since the crystal is 4 cm long and the assumed one-way optical power inside the resonator is 5 W, the absorbed power is 0.08 W. rf-heating can be estimated from the applied modulator voltage and the equivalent resistance characterizing the ohmic loss,

$$P_{rf,loss} = \frac{1}{2\pi f_B} \int_{f_1}^{f_1+f_B} \frac{df}{f\ C\ \tan\delta(f)}\ , \qquad (C1)$$

where f is the instantaneous frequency, f_1 the lower boundary and $f_1 + f_B$ the upper boundary of the chirp, C the modulator capacitance and δ the loss coefficient. The integral can be roughly approximated by inserting the midband value for frequency and loss, $\bar{f} = 2.5\ 10^8$, $\delta = 10^{-3}$ (Ref. 7), C = 15 pF, and V_{peak} = 235 V (Section 2.0). We obtain $P_{rf,loss} \approx 0.6$ W; i.e., for the maximum rf power, ohmic heating far exceeds optical heating of the modulator crystal. In order to keep the crystal at a relatively low temperature, which is desirable because of a reduction in the breakdown field strength with increasing temperature, efficient cooling is required.

APPENDIX D

POWER CONSIDERATIONS

The steady state behavior of a low gain CO_2 laser is described by

$$2g\ell\ (1 + 2P_i/P_s)^{-1} = \alpha + T, \qquad (D1)$$

where ℓ is the length of the plasma column; g the unsaturated exponential power gain coefficient per unit length of the active medium; P_i the intracavity power flow in one direction; P_s the saturation power; α the intracavity loss encountered upon a round-trip transmission through the resonator and T the relative transmission of the output mirror. Equation (D1) states that the power-saturated gain of the active medium has to compensate for the total optical loss consisting of output coupling and resonator losses (imperfect reflection at the mirrors, transition from free space to guided propagation, radiation leakage into the capillary wall, absorption in the modulator, and reflection off the modulator faces). The output power is given by $P_o = T \times P_i$, hence

$$P_o = T \cdot \tfrac{1}{2}P_s\,[2g\ell/(\alpha + T) - 1]. \qquad (D2)$$

Two different waveguide lasers now in operation at UARL, one open-cycle and one sealed-off, shall be considered.

The open-cycle system employs a BeO tube, approximately 10 cm long, with a 1.0 mm ID bore. CO_2, N_2 and He are mixed in the ratio 1:1:3 and flow through the plasma vessel into a mechanical vacuum pump. The main pressure drop occurs at the entrance and exit of the capillary while the pressure inside the capillary is nearly constant, assuming a value midway between the pressure values measured at the gas-intake and gas-exhaust ports. As the flow is increased from 10 to 35 std cm^3/sec, the concomitant capillary pressure rises from 40 to 150 torr. Since the capillary volume is 0.08 cm^3, a flow of 10 std cm^3/sec yields a 250 times/sec replacement of the active gas. The laser was operated with a HR concave mirror of 25 cm radius of curvature and a T = 7.6%, concave mirror with a radius of curvature of 20 cm yielding a maximum output power of 750 mW at 100 torr gas pressure and 20 deg tube temperature. Inserting the value $2g\ell = 0.42$ (measured), $\alpha = 0.08$ (estimated guiding and mirror losses per round trip) and T = 0.076 (measured), we calculate from Eq. (D2) an integrated saturation power of $P_s = 12.0$ W. The saturation intensity is $I_s = P_s/\pi\sigma^2$, where σ is the e^{-1} intensity radius of the gaussian beam which best matches the EH_{11} waveguide mode. This gives a value of $\sigma/a = 0.455$. Since $a = \frac{1}{2}$ mm, we find for the saturation intensity $I_s = 7.4$ kW/cm^2.

The second waveguide system, a sealed-off unit, uses a waveguide of 1.5 mm ID and 5 in. length. This system was filled with a gas mixture of He, N_2, CO_2, Xe and H_2 in the ratio 4:1:1:0.13:0.1 to a total pressure of 100 torr yielding a maximum power of 1.5 W at 20 deg tube temperature.

The power per unit volume of plasma column is 9.6 W/cm^2 for the open cycle and 6.8 W/cm^3 for the sealed-off system. Using the estimated value $g = 0.01/cm$, $\alpha = 0.04$ together with $\ell = 12.5$ cm, $T = 0.05$ and scaling the integrated saturation power with the capillary cross section, we calculate from Eq. (D2) an output power of 1.2 W for the sealed-off system which represents a reasonable agreement with the measured output in view of the uncertainty in the parameter values.